

Method to evaluate large wood behavior in terms of convection equation associated with sediment erosion and deposition

Daisuke HARADA¹, Shinji EGASHIRA¹

¹International Centre for Water Hazard and Risk Management (ICHARM), Public Works Research Institute (PWRI), 1-6, Minamihara, Tsukuba, Ibaraki, 305-8516, Japan

Correspondence to: Daisuke HARADA (d-harada55@pwri.go.jp)

Abstract. This paper proposes a method for describing large wood behavior in terms of the convection equation and the storage equation, which is associated with active sediment erosion and deposition. Recent flood hazards are characterized by numerous amounts of sediment and large wood supplied from upstream mountainous areas, which often exacerbate flood disasters in downstream areas. Previous studies proposed methods to simulate large wood behavior by tracking the motion of individual wood pieces in the flood flow using the Lagrangian method. This study proposes a new method to simulate the behavior of numerous large wood pieces in the flow field with active sediment transportation by employing the convection equation and the storage equation for large wood. The proposed method is applied to simulate the flood flow with numerous amounts of sediment and large wood in the Akatani river flood disaster event. The 2-D flood flow computations indicate that the flood flow can be significantly affected by the large wood deposition at the bridge in terms of water level, velocity distribution, and sediment deposition. The comparison between the field and simulation results shows the applicability of the proposed methods to evaluate large wood behavior where active sediment erosion and deposition occurs. Overall, since the proposed method makes it possible to simulate the behavior of a numerous number of large wood, it can be applied to the management of hazards in mountainous rivers such as the Akatani River.

1 Introduction

On July 5th, 2017, Northern Kyusyu in Japan experienced extremely heavy rainfall, which caused landslides and debris flows at numerous locations in its mountainous regions. In Japan, disasters caused by sediment and flood inundation are becoming increasingly apparent in mountainous areas or steep slope areas. This is caused by sediment and large wood pieces transported by landslides and debris flows associated with heavy rainfall and deposited at small valley outlets, eroded and transported by flood waters, and inundated with flood waters where the sediment transport capacity is rapidly reduced. The Akatani River, with a basin area of approximately 20 km², suffered particularly severe damage in this disaster (Chen et al., 2018; Harada and Egashira, 2018). The photo on the left side of Figure 1, taken immediately after the disaster, shows that the sediment and large wood produced by the debris flow were accumulated at the valley outlet. According to the results of the laser profiler survey, approximately 2.9 million m³ of sediment was produced in the Akatani River basin. Multiplying

30 the area of the landslide area by 549 m³/ha of timber volume per unit area, it is estimated that approximately 39,000 m³ of
large wood was supplied (MLIT, 2017). This means that assuming the standing tree density as one tree in 2m²,
approximately 19,500 pieces of large wood were produced during the event, from the Akatani river basin. A part of these
sediment and large wood were transported downstream by the flood flow. In downstream areas, large wood accumulated at
many locations, such as bridges, influencing the flood flow. The photo on the left side of Figure 1, taken immediately after
35 the disaster, shows that considerable amounts of large wood were accumulated at around the bridge.

Recently, these types of flood hazards have been reported to occur in many places of steep, forested areas (Lucía et al., 2015;
Lucía et al., 2018; Steeb et al., 2017; Comiti et al., 2016; Harada et al., 2019). As reported in those studies, large wood
pieces often become a major contributing factor that exacerbates flood disasters. Hence, it is highly important to develop a
method to evaluate their behavior in a flood flow.

40 Research on large wood in rivers has been conducted, and some studies have proposed simulation models for their behavior
(Swanson et al., 2021; Ruiz-Villanueva et al., 2019). Nakagawa et al. (1994) proposed a numerical simulation model to
compute the behavior of individual wood pieces in a two-dimensional flow field by calculating the transportation of
driftwood using a combination of translocation and rotation. This method was applied and verified in several laboratory
experiments (Shrestha et al., 2009; Shrestha et al., 2012). Gotoh (2001) proposed a method to track the motion of driftwood
45 based on the Lagrange particle method (MPS method) by treating wood pieces as rigid bodies. Shimizu et al. (2006)
developed a model composed of two types of analyses: the Eulerian analysis of fluid motion, using depth-averaged flow
analysis, and the Lagrange analysis of driftwood motion, using the extended distinct element method. Ruiz-Villanueva et al.
(2014) proposed a method to compute the transport of individual large wood pieces in a two-dimensional flow field,
including physical modeling of the wood recruitment process to the flood flow. Kimura et al. (2021) developed models to
50 compute large wood motion in a three-dimensional flow field.

In addition to those proposed methods for the behaviour of wood pieces in a flow field, some research proposed methods to
analyse large wood production processes from a watershed. Benda and Sias (2003) proposed stochastic methods to predict
long term wood budgets in watersheds. Mazzorana et al. (2009) proposed methods to estimate large wood production
processes in mountainous streams by a GIS-based index. Mazzorana et al. (2011) proposed a model for wood entrainment
and deposition processes based on empirical methods and the transportation of wooden materials in the flow field. Komori et
55 al. (2021) proposed a model to evaluate large wood export at a watershed scale.

In order to evaluate sediment and flood inundation phenomena including a numerous amount of wood pieces, it is important
to properly evaluate the processes from the occurrences of landslides and debris flows to their depositions on hillslopes and
small streams. These can now be evaluated using slope and topsoil layer models, channel network models, rainfall-runoff
60 models, and mass point, one-dimensional and bathymetrically averaged two-dimensional analytical models for sediment and
large wood (Yamazaki and Egashira, 2019)

In addition to these studies, empirical relations have also been investigated for large wood runoff during heavy rainfall
events. However, in flood disasters such as the Akatani River, considerable amounts of sediment and large wood were

65 produced due to occurrences of landslides and debris flows in mountainous areas during a few hours of rainfall, immediately transported downstream by flood flows and contributed to the flood disaster. The basin had not been experienced such disasters in the history of observation records. In order to mitigate the damage of such disasters, structures to capture large wood are being planned in several Japanese rivers. To evaluate their effectiveness, it is necessary to evaluate the spatio-temporal distribution of large wood discharge, i.e., the amount of sediment and large wood at an arbitrary location in the river channel, and to evaluate the impact of large wood in the flow field with active sediment transportation and bed deformation. The present paper proposes a numerical method to describe the behavior of large wood pieces based on a convection equation and a storage equation considering sediment erosion and deposition. Then, calculating flood flows downstream using a 2-D depth-integrated flow model with sediment and large wood, we investigate how large wood behavior, e.g., wood capture at bridges, may affect flood flows and sediment deposition in the surrounding area. The proposed model has been applied to the 2017 flood disaster in Northern Kyusyu to understand the effect of large wood behavior on the flood flow.

2 Methods

In our proposed methods, the flow field is simulated using 2-D depth-integrated governing equations, which include mass and momentum conservation equations. The equations are expressed in the Cartesian coordinate system as follows:

$$\frac{\partial h}{\partial t} + \frac{\partial uh}{\partial x} + \frac{\partial vh}{\partial y} = 0 \quad (1)$$

$$\frac{\partial hu}{\partial t} + \frac{\partial huu}{\partial x} + \frac{\partial huv}{\partial y} = -gh \frac{\partial(h + z_b)}{\partial x} - \frac{\tau_x}{\rho} + \frac{1}{\rho} \left(\frac{\partial h \sigma_{xx}}{\partial x} + \frac{\partial h \tau_{yx}}{\partial y} \right) \quad (2)$$

$$\frac{\partial hv}{\partial t} + \frac{\partial huv}{\partial x} + \frac{\partial hvv}{\partial y} = -gh \frac{\partial(h + z_b)}{\partial y} - \frac{\tau_y}{\rho} + \frac{1}{\rho} \left(\frac{\partial h \tau_{xy}}{\partial x} + \frac{\partial h \sigma_{yy}}{\partial y} \right) \quad (3)$$

70 where x and y are the coordinates in the major flow direction and normal to the flow direction, respectively; t is the time; h is the flow depth; u and v are the x and y components of the depth-averaged velocity; g is the acceleration due to gravity; ρ is the mass density of water; σ_{xx} , σ_{yy} , τ_{xy} , and τ_{yx} , are the depth-averaged Reynolds stresses; z_b is the bed elevation; τ_x and τ_y are the x and y components of the bed shear stress, respectively.

Equations (1) to (3) are transformed into a general coordinate system (Shimizu and Itakura, 1991). The equations are numerically calculated by the cubic interpolated pseudo-particle (CIP) method (e.g., Yabe et al., 1991, Jang and Shimizu, 85 2005).

The processes of bed deformation and suspended sediment transport in the flow field are computed using the following equations:

$$\frac{\partial z_b}{\partial t} + \frac{1}{1 - \lambda} \sum_i \left(\frac{\partial q_{bix}}{\partial x} + \frac{\partial q_{biy}}{\partial y} + E_i - D_i \right) = 0 \quad (4)$$

$$\frac{\partial c_i h}{\partial t} + \frac{\partial u c_i h}{\partial x} + \frac{\partial v c_i h}{\partial y} = E_i - D_i \quad (5)$$

where λ is the porosity of the bed sediment; q_{bix} and q_{biy} are the x and y components of the bedload transport rate for grain size d_i , respectively, E_i and D_i are the erosion and deposition rates of the suspended sediment for grain size d_i , respectively, c_i is the depth-averaged suspended sediment concentration for grain size d_i .

The bedload transport rate is estimated using a formula developed by Egashira et al. (1997), in which the constitutive relations of a water-sediment mixture flow are applied to the bedload layer.

$$q_{b*i} = \frac{4}{15} \frac{K_1^2 K_2}{\sqrt{f_d + f_f}} \tau_{*i}^{5/2} p_i \quad (6)$$

where q_{b*i} is the non-dimensional bedload transport rate for grain size d_i ; τ_{*i} is the non-dimensional tractive force for grain size d_i ; p_i is the content ratio for grain size d_i ; the other parameters, K_1 , K_2 , f_d , and f_f , are specified based on Egashira et al. (1997).

$$K_1 = \frac{1}{\cos \theta} \frac{1}{\tan \phi_s - \tan \theta} \quad (7)$$

$$K_2 = \frac{1}{\bar{c}_s} \left[1 - \frac{h_s}{h} \right]^{1/2} \quad (8)$$

$$f_d = k_d (1 - e^2) \frac{\sigma}{\rho} \bar{c}_s^{-1/3} \quad (9)$$

$$f_f = k_f (1 - \bar{c}_s)^{5/3} \bar{c}_s^{-2/3} \quad (10)$$

where θ is the local slope; ϕ_s is the angle of repose; \bar{c}_s is the sediment concentration on the bedload layer; h is the water depth; σ is the density of soil particle; ρ is the density of water; e is the coefficient of restitution; $k_d=0.0828$; $k_f=0.16 \sim 0.25$. Indeed, most of the values in equations (7) to (10) are regarded as constant in the flow field described by equations (1) to (3), thus assuming, $\phi_s = 34^\circ$, $\bar{c}_s = 0.25$, and $h_s \approx h$, the value of the term $4/15 K_1^2 K_2 / \sqrt{f_d + f_f}$ in equation (6) is approximately 3.8.

In equation (8), h_s is the thickness of the bedload layer, which is described as follows:

$$\frac{h_s}{h} = \frac{1}{\left(\frac{\sigma}{\rho} - 1\right) \bar{c}_s} \frac{\tan \theta}{\tan \phi_s - \tan \theta} \quad (11)$$

The grain size distribution of bed materials is evaluated based on the concept of the bedload layer, the transition layer, and the deposition layer, which was developed by Luu et al. (2006), assuming that the mass of each material is preserved.

Erosion rate E_i of suspended sediment in equations (4) and (5) are evaluated using the following equations proposed by Harada et al. (2022);

$$E_i = p_i W_e \bar{c}_s \quad (12)$$

$$\frac{W_e}{U} = \frac{K}{R_{i*}} \quad (13a)$$

$$R_{i*} = (\sigma/\rho - 1)\bar{c}_s gh/U^2 \quad (13b)$$

where W_e is the entrainment velocity, U is the flow velocity, i.e., $x = \sqrt{u^2 + v^2}$, R_{i*} is the overall Richardson number, c is the depth-averaged suspended sediment concentration, and $K = 1.5 \times 10^{-3}$ (Egashira and Ashida, 1980).

To analyze considerable amounts of large wood in the flood flow, it is assumed that wood pieces behave as neutral buoyant particles, for this assumption enables the introduction of the convection equation. Further, assuming that the erosion and
 110 deposition of large wood take place in proportion to sediment erosion and deposition and also assuming that large wood accumulation occurs at artificial structures such as bridges, the convection equation is coupled with the storage equation of large wood in the channel bed. **This concept is based on the situation that considerable amount of sediment and large wood were deposited where the sediment transport capacity was suddenly decreased in the flow direction in places such as fan topography formed by debris flow, as shown in the left photo in Figure 1.**

115 Based on these assumptions, the behavior of large wood in the flood flow is expressed using the following equations:

$\partial z_b/\partial t > 0$:

$$\frac{\partial c_{drf} h}{\partial t} + \frac{\partial c_{drf} u h}{\partial x} + \frac{\partial c_{drf} v h}{\partial y} = -c_* \frac{\partial z_b}{\partial t} c_{drf} r(t, x, y) - v_n c_{drf} p_b \delta(x - x_i, y - y_i) \quad (14)$$

$$\frac{\partial S}{\partial t} = \frac{\partial z_b}{\partial t} c_{drf} r(t, x, y) + v_n c_{drf} p_b \delta(x - x_i, y - y_i) \quad (15)$$

$\partial z_b/\partial t < 0$:

$$\frac{\partial c_{drf} h}{\partial t} + \frac{\partial c_{drf} u h}{\partial x} + \frac{\partial c_{drf} v h}{\partial y} = -c_* \frac{\partial z_b}{\partial t} \frac{S}{D} r(t, x, y) - v_n c_{drf} p_b \delta(x - x_i, y - y_i) \quad (16)$$

$$\frac{\partial S}{\partial t} = \frac{\partial z_b}{\partial t} \frac{S}{D} r(t, x, y) + v_n c_{drf} p_b \delta(x - x_i, y - y_i) \quad (17)$$

where c_{drf} is the depth-averaged large wood concentration; c_* is the sediment concentration of the stationary bed; v_n is the inward velocity normal to the structure area such as the bridge; D is the depth of the standing tree's root; S is the storage of
 120 large wood on the ground or the riverbed per unit area; when the volume of a piece of wood is V (m^3), S and the number of wood (N) in a certain area (A m^2) is converted by $S = VN/A$ (m).

Equations (14) and (16) are the convection equations for large wood transport with the water flow, and equations (15) and (17) are the storage equations of large wood stored on the bed. The first term of the right-hand side in equations (14) to (17) represents the large wood exchange between the water and the bed. Since we assume that the erosion and deposition of large
 125 wood take place in proportion to sediment erosion and deposition, the term in equations (14) and (15) represents the wood deposition from the water to the bed, and the term in equations (16) and (17) represents the large wood recruitment from the bed to the water. Figure 2 (a) shows the concept of these processes.

In the case of sediment deposition, $c_* \partial z_b / \partial t$ corresponds to the height of sediment deposition per unit time. We assume that large wood pieces within the height range are deposited to the riverbed; thus, the amount of $c_* \partial z_b / \partial t c_{drf}$ is stored in the riverbed. In the case of sediment erosion, as shown in Figure 2 (b), when the bed erosion reaches root depth D , all wood storage S is recruited to the water. Therefore, $S c_* \partial z_b / \partial t / D$ corresponds to the large wood recruitment from the bed to the water per unit time.

Meanwhile, large wood recruitment does not occur at depths shallower than a certain water depth, and large wood deposition does not occur at depths deeper than a certain water depth. Function $r(t, x, y)$ in equations (14) to (17) is introduced to describe these cases and set as shown in Figure 3 in the present research.

In equations (14) and (16), the last term defines large wood capture at the structures. Dirac's δ -function is employed to evaluate the capturing of large wood at structures such as bridges by defining the locations of these types of structures as $((x, y) = (x_i, y_i))$ and setting Dirac's δ -function for the structures as $\delta = 1$ and for other places as $\delta = 0$. p_b denotes the probability that large wood is captured at structures, ranging from 0 to 1.

When large wood deposition occurs, the sediment transport rate may be reduced due to the hidden effect of large wood deposition. Therefore, in the present study, the bedload transport rate in equation (6) and the erosion rate of suspended sediment in equation (12) are reduced at the rate of the hidden effect.

At a point where a structure, such as a bridge, exists, e.g., $((x, y) = (x_i, y_i))$, the water decreases in the cross section where the velocities across the cell, i.e., $u\Delta x$ and $v\Delta y$, are reduced by $u\alpha\Delta x$ and $v\alpha\Delta y$, in which α is described as follows:

$$\alpha = \frac{S}{h} / (1 - c_{*drf}) \quad (18)$$

where c_{*drf} is the wood concentration of a stationary layer composed of the deposited large wood only.

3 Numerical simulations

3.1 Target areas and hazard characteristics

Numerical simulations of a flood flow with sediment and large wood are conducted for the Akatani River basin, which is located on the right-bank side of the Chikugo River, where a large amount of sediment and large wood was produced in the 2017 flood disaster in Northern Kyusyu, Japan. The drainage area and the stream length of the Akatani River are approximately 20 km² and 8 km, respectively. According to Nagumo & Egashira (2019), 639 houses or buildings in the basin were damaged during the event. Figure 4 shows the Akatani River basin with debris flows and flood marks identified from aerial photos. This shows that numerous landslides and debris flows occurred in the mountainous areas, which increased damage to the downstream areas. Figure 5 compares aerial photos taken before and after the disaster. Although it is difficult to identify the river channel in the photo before the event because of its very narrow width, the photo after the event clearly shows sediment widely spreading over the valley bottom, indicating highly active sediment transport and deposition during the event.

Figure 6 shows the sediment size distribution observed immediately after the flood event. Longitudinal sediment sorting is clearly observed, exhibiting a tendency for the sediment size to become finer downstream. Moreover, although the average bed slope of the entire Akatani River channel is approximately 1/70, the grain size of the deposited sediment is quite fine, which indicates that a large amount of fine sediment was supplied from the upstream area during the event.

During the flood event, numerous amounts of large wood were supplied to the channels. Figure 7 shows the distribution of deposited wood length, which is identified from aerial photos taken just after the event. Three areas along the Akatani River channel and one valley in the basin shown in Figure 4 are selected to investigate the length of each wood piece, for the resolution of the aerial photos taken for these areas is sufficient for this purpose. According to Figure 7, the distribution of wood length decreases from the inside of the valley to its outlet. A part of the large wood deposited in the outlet of the valley may have been transported to downstream due to the flood flow and deposited along the Akatani River channel.

3.2 Upstream boundary conditions

To conduct a 2-D depth-integrated analysis under the conditions such as the Akatani River disaster, it is necessary to evaluate the amount of sediment and large wood inflow from the basin at the upstream boundary of the 2-D analysis area. In this study, we obtained the upstream boundary condition by an integrated method to simulate rainfall-runoff, landslide and debris flow, and sediment and large wood transport in the river channel to obtain a time series of sediment and large wood discharged from the basin.

The Rainfall-runoff-inundation (RRI) model, developed by Sayama et al., (2012), is prepared for the entire basin. The model deals with slopes and river channels separately. The flow on the slope grid cells is calculated with the 2D diffusive wave model, while the channel flow is calculated with the 1D diffusive wave model. On the slope grid cells, the slope stability analysis and debris flow computations (Yamazaki et al., 2016, Yamazaki and Egashira, 2019) are conducted. The occurrence of landslides is determined using the balanced equation of a force's action on an infinite slope. When the landslide occurrence is detected, the surface soil in the cell is transported from the point of origin to the location where the deposition occurs, using the equation of a mass system. Along with the sediment transport due to the landslide and debris flow, the standing woods there is also recruited to the debris flow, and transported following the one-dimensional notation of equations (14) to (17).

When the debris flow reaches the river channel grid cells, sediment and large wood are treated as sediment and large wood supply to the river channel. In the river channel grid cells, sediment and large wood transport is evaluated with the methods proposed by Egashira and Matsuki (2000), in which a section that includes the upstream confluence and excludes the downstream confluence point is designated as the unit channel, and the sediment and large wood runoff for the entire basin is predicted by allocating the unit channels in series and parallel. As for the large wood transport in the channel network, the behavior of the large wood in the unit channel follows the one-dimensional forms of equations (14)-(17).

These models are applied to the Akatani River event in 2017 to estimate the time series of water, sediment, and large wood discharged from the basin. JMA analytical rainfall data is given as the rainfall data for the model. Since there is no

hydrological record in the Akatani River basin, the model parameters were validated using the Kagetsu river basin data, which locates east of the study basin. As a result, we estimate the peak discharge as approximately 340 (m³/s) at the 3.5 km point; the location corresponds to the upstream boundary of the 2-D flood flow computation, which is close to those of Shakti et al. (2018) (400 m³/s) and the Ministry's reports (MLIT, 2017) (400 m³/s).

195 Parameters employed for the rainfall-runoff and landslide calculations are shown in Table 1. As for the landslide and debris flow, model parameters are validated so that sediment transport locations and its total areas are close to those of Figure 4 and the Ministry's reports (MLIT, 2017). The initial conditions of sediment size distribution in the river channel are shown by the red dotted line in Figure 6. As for the large wood runoff computation from the basin, referring to our surveys and Kubota (2019), the density of standing trees is set as 0.06 (m³/m²), assuming that the average diameter of a standing tree is 15 cm, 200 the length 11.2 m, and the density per standing tree 2 m².

The upstream boundary conditions obtained using this method are shown in Figure 8. The Figure shows the temporal variation of the basin scale computational results for flood water, suspended sediment, and large wood discharge at the 3.5 km point; the location corresponds to the upstream boundary of the 2-D flood flow computation. According to the figure, suspended sediment and large wood discharge are concentrated before the flow discharge peak comes.

205 3.3 Computational conditions for the 2-D flood flow with sediment and large wood behavior

The computation area is approximately 3.5 km long, as shown in Figure 4. The average bed slope of the computational domain within the 3.5km is approximately 1/120. For the computation, iRIC-Nays2DH (Shimizu et al., 2019), which was partially modified by the authors, is employed. As the initial topography, DEM data measured by an aerial laser survey before the flooding are used. The roughness coefficient is set as 0.03 for the entire computation domain, which was 210 determined so that the flood marks would match the computation results. The initial sediment size distribution, indicated by the red dotted line in Figure 6, is given for the entire computed domain. No large wood is assumed to be initially deposited (S=0 in Eqs. (14)-(17)) in the entire calculation domain.

Seven bridges inside the domain were set as obstacles, and $\delta = 1$ in equations (14)-(17) at these locations. The large wood capture rate p_b at bridges can take values between 0 and 1, but in this study, p_b is uniformly set to 1. In this computation, 215 when large wood accumulation takes place on bridges, the cross-section area of the flow in the grid is reduced, which in turn affects the flow conditions around the bridges. Calculations are performed for the three cases shown in Table 2 to compare the differences in results depending on the presence of sediment and large wood. Case 1 is the flow computation only without sediment and large wood, Case 2 is the flow with sediment without large wood, and Case 3 is the flow with sediment and large wood.

220 4 Computation results

Figure 9 compares Cases 1, 2, and 3, and shows a water depth contour map at the peak discharge time, which shows the area between 1.2 km and 2.5 km from the downstream end of the computational domain. For example, the area circled by the solid white line in Figure 9 shows that a wider area is inundated in Case 3 than in Case 1, which is closer to the actual inundated area.

225 Figure 10 compares the difference between the ground elevation measured by an aerial laser survey before and after the flooding (left figure) and the difference between the beginning and the end of the calculation for the ground elevation in Case 3 (right figure). Although the calculation results show a little excessive sediment deposition upstream of the 1.5 km point, the two trends are generally consistent in that more than 2m sediment deposition takes place in the river channel and that sediment is deposited several tens of centimeters to 1m thick in the areas where inundation occurred.

230 Figure 11 compares the observed number of large-wood pieces deposited in a 25-m square area with the number of computed pieces deposited at the end of the calculation. The number of observed large wood pieces deposited within a 25-m square area is determined from aerial photographs taken immediately after the flood event. The computed results, i.e., S in equations (14)-(17), are converted to the number of large wood pieces by assuming that the diameter and length of a piece of wood are 20 cm and 7 m, respectively, referring to Figure 7 and Kubota (2019). According to the figure, although it should
235 be noted that some of the large wood pieces may be undecipherable because it is buried and not surfaced though being deposited, the trend of large wood deposition in the area is generally consistent.

5 Discussions

This section provides a more detailed discussion concerning the impact of large wood on flood flows, and the characteristics of the method proposed in this study.

240 Figure 11 shows the water level in the river channel and the riverbed height at the peak flow in three different cases and compares the results with the trace water level. In Case 3, the accumulation of large wood near the bridge obstructs the river channel flow; thus, the water level rises markedly upstream of the bridge. Comparing the trace water level and the calculated water level around the 1.5 km point, the water levels in Cases 1 and 2 are about 1 m lower than the trace water level, and the water level in Case 3 is partly due to the large wood capture rate p_b at the bridge is uniformly set to 1, but at least the
245 water level is evaluated lower in Cases 1 and 2, where large wood is not considered. In Case 3, the bed shear stress in the river channel is reduced at upstream of the bridge, that causing significant sediment deposition here.

Figure 12 shows that in Case 3, a large amount of sediment has already been deposited in the river channel before the peak flow, which significantly reduces the channel capacity before the peak flow. In Case 2, the sediment deposition in the river channel is also significant; however, the amount of sediment deposition is not as large as in Case 3 because the deposition of
250 large wood at the bridge and the associated flow obstructions are not calculated. Due to these effects, the flood inundation expands over the valley bottom, as is especially noticeable near the bridge in Case 3 in Figure 9.

Figure 13 shows the contours of the flow velocity in the vicinity of the bridge (1.2 to 1.5 km). Figure 13 compares Case 2, in which large wood is not computed, with Case 3, in which large wood is computed. The flow is obstructed in the bridge due to the large wood accumulation at the bridge, causing the flow to divert around it. This results in a larger area of inundation in Case 3 and a larger area subject to higher velocity fields.

With regard to the spatial distribution of large wood deposition, the difference between the left and right figures of Figure 11 shows the correspondence between the observation and calculation results of large wood. In area (b), where large wood tends to accumulate near the bridge, the observed and calculated results correspond to some extent. On the other hand, in area (a), the observation results show that large wood is deposited far from the original river channel, while the calculation results show that large wood is deposited close to the original river channel, i.e., the right side of the white dotted rectangle. In this area, the flow that is separated from the main flow becomes an eddy and deposits suspended sediment and large wood at far from the original river channel, whereas the phenomena is not well reproduced in the computation due to the issue of grid scale. Since the present method assumes the large wood deposition occurs where sediment deposits as described in equations (14) and (15), the reproductivity of bed deformation greatly influences the results of large wood deposition.

The present paper has proposed a new approach to simulate the behavior of large wood in the flow field based on the convection-diffusion equation. The approach is particularly useful for cases requiring a considerable number of large wood behavior simulations because it is impractical to employ the Lagrangian approach when considerable amounts of large wood are supplied, as in the case of the Akatani River. The method is also beneficial in simulating large wood accumulation at structures such as bridges. On the other hand, since the deposition of large wood on a riverbed and the amount of large wood captured by bridges depend on functional form $r(t, x, y)$ and capture rate p_b , the method for setting these parameters should be studied further. In other words, the exchange of large wood from the water to the riverbed or from the water to the bridge also requires further research for application.

6 Conclusion

The present paper has proposed a method to simulate the behavior of large wood in the flow field based on the convection equation and the storage equation with active sediment transportation and channel bed deformation, which characterizes recent flood disasters in mountainous and hilly regions, such as the flood disaster in the Akatani river in 2017. The proposed method is applied to simulate the flood flow with numerous amounts of sediment and large wood in the Akatani river flood disaster.

From the results of 2-D flood flow computations with sediment and large wood, we found that the large wood deposition is reproduced where bed deformation is well reproduced. The calculation results are significantly different when the effects of sediment and large wood are considered, indicating that it is essential to consider these factors in the analysis. In particular, when large wood is captured in a bridge, the obstruction of the flow causes the flow diversion around the bridge, which significantly affects the flow pattern and river bed deformations above around the bridge. In this model, the erosion and

deposition of large wood, as well as the large wood capture rate at the bridge, are factors that significantly affect the
285 calculation results and these will require further study.

Since the proposed method makes it possible to simulate the behavior of a large number of driftwood pieces, it can be
applied to the management of hazards, such as the Akatani river. The computed results are useful for obtaining the
effectiveness of countermeasures, developing hazard maps, and evacuation plans. In addition, the effect of countermeasures
such as large wood capturing structures can be evaluated through simulations using the proposed method, which provides
290 practical information to control hazards more efficiently and effectively.

Data availability

The data used in this study are freely available from the corresponding author upon request.

Author contributions

DH and SE designed the study. DH performed the numerical simulations, and wrote the paper. SE reviewed and edited the
295 paper.

Competing interests

The authors declare that they have no conflict of interest.

Acknowledgements

The authors would like to thank Dr. Nagumo, N., Mr. Nakamura, Y. and Dr. Yamazaki, Y. for their contribution to field
300 survey and data preparation.

Financial support

This work was supported by JSPS KAKENHI Grant Number 22K14334.

References

Benda, L. E., Sias, J. C.: A quantitative framework for evaluating the mass balance of in-stream organic debris. *Forest
305 Ecology and Management*, 172, pp.1–16, doi:10.1016/S0378-1127(01)00576-X, 2003.

- Chen, X., Hirakawa, R., & Ohmoto, T.: Numerical Analysis of Effect of Bridge on Inundation Flow in the Kagetsu River on July 2017. *International Journal of Environmental Protection and Policy*, 6(4), 78-84. doi: 10.11648/j.ijep.20180604.12, 2018.
- Comiti, F., Lucía, A., & Rickenmann, D.: Large wood recruitment and transport during large floods: a review. *Geomorphology*, 269, 23-39, doi:10.1016/j.geomorph.2016.06.016, 2016.
- 310 Egashira, S., and Ashira, K.: Studies on the Structures of Density Stratified Flows., *Bulletin of the Disaster Prevention Research Institute, Kyoto University*, 29(4), pp.165-198, 1980.
- Egashira, S. and Matsuki, T.: A method of predicting sediment runoff caused by erosion of stream channel bed. *Annual Journal of Hydraulics Engineering, Japan Society of Civil Engineers*, 44, 735–740, 2000 (In Japanese).
- 315 Gotoh, H.: Sub-particle-scale turbulence model for the MPS method-Lagrangian flow model for hydraulic engineering. *Computational Fluid Dynamics Journal*, 9(4), pp.339-347, 2001.
- Harada, D. & Egashira, S.: Flood flow characteristics with fine sediment supply and drift woods -analysis on the akatani river flood hazards in july, 2017-, *Annual Journal of Hydraulic Engineering, JSCE*, vol.74: I_937-I_942, 2018 (In Japanese).
- Harada, D., Nagumo, N., Nakamura, Y., Egashira, S.: Characteristics of Flood Flow with Active Sediment Transport in the Sozu River Flood Hazards at the Severe Rainfall Event in July 2018., *Journal of Disaster Research* 14.6, pp.886-893, doi:10.20965/jdr.2019.p0886, 2019.
- 320 Harada, D., Egashira, S., Ahmad, T. S., & Ito, H.: Entrainment of bed sediment composed of very fine material, *Earth Surface Process and Landforms*, Advance online publication. doi:10.1002/esp.5442, 2022.
- Harada, D., & Egashira, S.: Methods to analyse flood flow with a huge amount of sediment and driftwood, *Advances in river engineering, JSCE*, 28, 289-295, 2022 (In Japanese).
- 325 Jang, C. L., & Shimizu, Y.: Numerical simulations of the behaviour of alternate bars with different bank strengths. *Journal of Hydraulic Research*, 43(6), 596-612, doi:10.1080/00221680509500380, 2005.
- Kimura, I., Kang, T., & Kato, K.: 3D–3D Computations on Submerged-Driftwood Motions in Water Flows with Large Wood Density around Driftwood Capture Facility. *Water*, 13(10), 1406, doi:10.3390/w13101406, 2021.
- 330 Komori, D., Sukegawa, Y., Chaithong, T., & Kazama, S.: Modelling of large wood export at a watershed scale. *Earth Surface Processes and Landforms*, 47(2), 688-696, doi:10.1002/esp.5282, 2022.
- Kubota, T.: Elucidation of the Characteristics of Forest Slope Landslides and Woody Debris Disaster Induced by the Northern Kyushu Big Downpours in 2017. *Water science*, 62(6), 10-12, doi:10.20820/suirikagaku.62.6_10, 2019, (In Japanese).
- 335 Lucía, A., Comiti, F., Borga, M., Cavalli, M., & Marchi, L. Dynamics of large wood during a flash flood in two mountain catchments. *Natural Hazards and Earth System Sciences*, 15(8), pp.1741-1755. doi:10.5194/nhess-15-1741-2015, 2015.
- Lucía, A., Schwientek, M., Eberle, J., & Zarfl, C.: Planform changes and large wood dynamics in two torrents during a severe flash flood in Braunsbach, Germany 2016. *Science of the Total Environment*, 640, pp.315-326, doi:10.1016/j.scitotenv.2018.05.186, 2018.

- 340 Luu, X. L., Egashira, S., & Takebayashi, H.: A new treatment of the exchange layer thickness to evaluate sediment sorting and armoring. *Journal of applied mechanics*, 9, 1025-1030, doi:10.2208/journalam.9.1025, 2006.
- Mazzorana, B., Zischg, A., Largiader, A., & Hübl, J.: Hazard index maps for woody material recruitment and transport in alpine catchments. *Natural Hazards and Earth System Sciences*, 9(1), 197-209, doi:10.5194/nhess-9-197-2009, 2009.
- Mazzorana, B., Hübl, J., Zischg, A. M., Largiader, A.: Modelling woody material transport and deposition in alpine rivers, 345 *Natural Hazards* 56(2): 425–449, doi:10.1007/s11069-009-9492-y, 2011.
- MLIT (Ministry of Land, Infrastructure, & Transport): Report of the Technical Review Committee for River and Erosion Control Restoration in the Right Bank Basin of the Chikugo River, 2017.
- Nakagawa H., Takahashi T., and Ikeguchi M.: Numerical simulation of drift wood behavior. *Disaster Prevention Research Institute Annuals*, Vol. 35 B-2, pp. 249-266, 1994 (In Japanese).
- 350 Nakamura, Y., Ikeuchi, K., Abe, S., Koike, T., & Egashira, S.: Evaluation of the uncertainty of flash flood prediction using the RRI model in mountainous rivers. *EPiC Series in Engineering*, 3, 1486-1494, doi:10.29007/n72w, 2018.
- Nagumo, N. & Egashira, S.: Flood Hazard Analysis and Locations of Damaged Houses Based on Land Classification in the Akatani River Basin Following Torrential Rainfall in Northern Kyushu, 2017, *Journal of Geography (Chigaku Zasshi)* ,128 (6) , pp.835-854, doi:10.5026/jgeography.128.835, 2019 (In Japanese).
- 355 Ruiz-Villanueva, V., Bladé, E., Sánchez-Juny, M., Marti-Cardona, B., Díez-Herrero, A., & Bodoque, J. M.: Two-dimensional numerical modeling of wood transport. *Journal of Hydroinformatics*, 16(5), 1077-1096, doi:10.2166/hydro.2014.026, 2014.
- Ruiz-Villanueva, V., Mazzorana, B., Bladé, E., Bürkli, L., Iribarren-Anacona, P., Mao, L., Nakamura, F., Ravazzolo, D., Rickenmann, D., Sanz-Ramos, M. and Stoffel, M.: Characterization of wood-laden flows in rivers. *Earth Surface Processes and Landforms*, 44(9), pp.1694-1709, doi:10.1002/esp.4603, 2019.
- 360 Sayama, T., Ozawa, G., Kawakami, T., Nabesaka, S., & Fukami, K.: Rainfall–runoff–inundation analysis of the 2010 Pakistan flood in the Kabul River basin. *Hydrological Sciences Journal*, 57(2), 298-312, doi:10.1080/02626667.2011.644245, 2012.
- Shakti P.C., Nakatani, T., & Misumi, R.: Hydrological simulation of small river basins in northern Kyushu, Japan, during the extreme rainfall event of July 5–6, 2017. *Journal of Disaster Research*, 13(2), 396-409, doi:10.20965/jdr.2018.p0396, 2018.
- 365 Shrestha, B. B., Nakagawa, H., Kawaike, K., Baba, Y., & Zhang, H.: Numerical simulation on debris-flow with driftwood and its capturing due to jamming of driftwood on a grid dam. *Annual Journal of Hydraulic Engineering, JSCE*, 53, 169-174, 2009.
- Shrestha, B. B., Nakagawa, H., Kawaike, K., Baba, Y., & Zhang, H.: Driftwood deposition from debris flows at slit-check 370 dams and fans. *Natural Hazards*, 61(2), 577-602, doi:10.1007/s11069-011-9939-9, 2012.
- Shimizu, Y., & Itakura, T.: Calculation of flow and bed deformation with a general non-orthogonal coordinate system, *Proceedings of XXIV IAHR Congress, Madrid, Spain, C-2* , pp. 41-48, 1991.

- Shimizu, Y., Nelson, J., Arnez Ferrel, K., Asahi, K., Giri, S., Inoue, T., Iwasaki, T., Jang, C.L., Kang, T., Kimura, I. and Kyuka, T.: Advances in Computational Morphodynamics Using the International River Interface Cooperative (iRIC) Software. *Earth Surface Processes and Landforms*, 45(1), 11-37, doi:10.1002/esp.4653, 2019.
- 375 Shimizu, Y., Osada, K., & Takanashi, T.: Numerical simulation of the driftwoods behavior by using a DEM-FLOW coupling model. *Annual Journal of Hydraulic Engineering, JSCE*, vol. 50, 787-792, 2006, (In Japanese).
- Steeb, N., Rickenmann, D., Badoux, A., Rickli, C., & Waldner, P.: Large wood recruitment processes and transported volumes in Swiss mountain streams during the extreme flood of August 2005. *Geomorphology*, 279, 112-127, doi: 10.1016/j.geomorph.2016.10.011, 2017.
- 380 Swanson, F. J., Gregory, S. V., Iroumé, A., Ruiz-Villanueva, V., & Wohl, E.: Reflections on the history of research on large wood in rivers. *Earth Surface Processes and Landforms*, 46(1), 55-66, doi: 10.1002/esp.4814, 2021.
- The River Sabo Technical Review Committee for the restoration on the Chikugo river right bank basin, Report on the Akatani river basin disaster, pp.67, 2018.
- 385 Yabe, T., Aoki, T., Sakaguchi, G., Wang, P. Y., & Ishikawa, T.: The compact CIP (Cubic-Interpolated Pseudo-particle) method as a general hyperbolic solver. *Computers & Fluids*, 19(3-4), 421-431, 1991.
- Yamazaki, Y., Egashira, S., & Iwami, Y.: Method to Develop Critical Rainfall Conditions for Occurrences of Sediment-Induced Disasters and to Identify Areas Prone to Landslides, *Journal of Disaster Research*, 11(6), pp.1103-1111, 2016.
- Yamazaki, Y., & Egashira, S.: Run out processes of sediment and woody debris resulting from landslides and debris flow. Association of Environmental and Engineering Geologists; special publication 28, doi:10.25676/11124/173184, 2019.
- 390



395 **Figure 1: Large wood deposition at the outlet of a valley bottom (left) and large wood depositions at around the bridges (right) in the Akatani river flood disaster, 2017.**

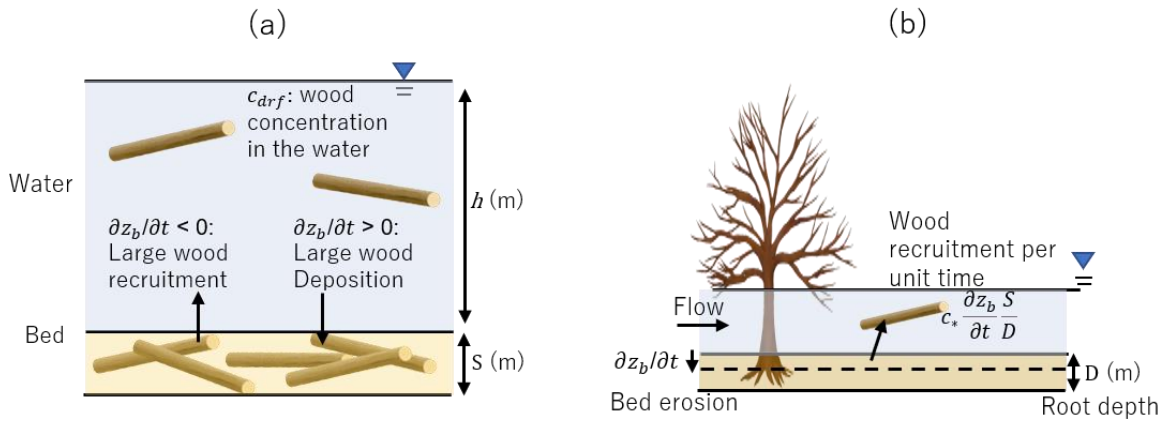
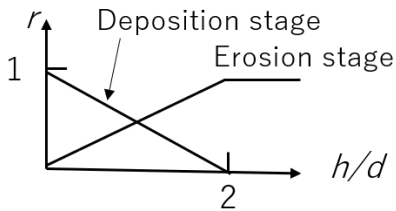


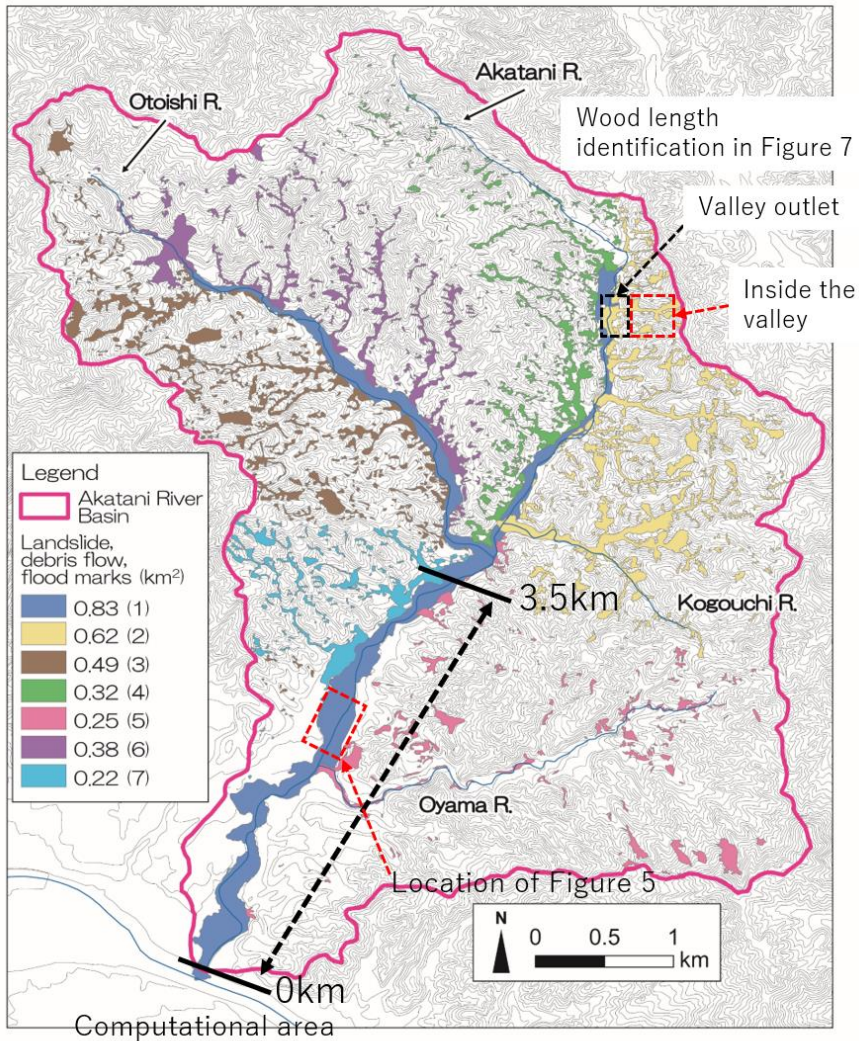
Figure 2: Concept of large wood recruitment and deposition (a), and the relation between bed erosion, root depth and large wood recruitment (b).



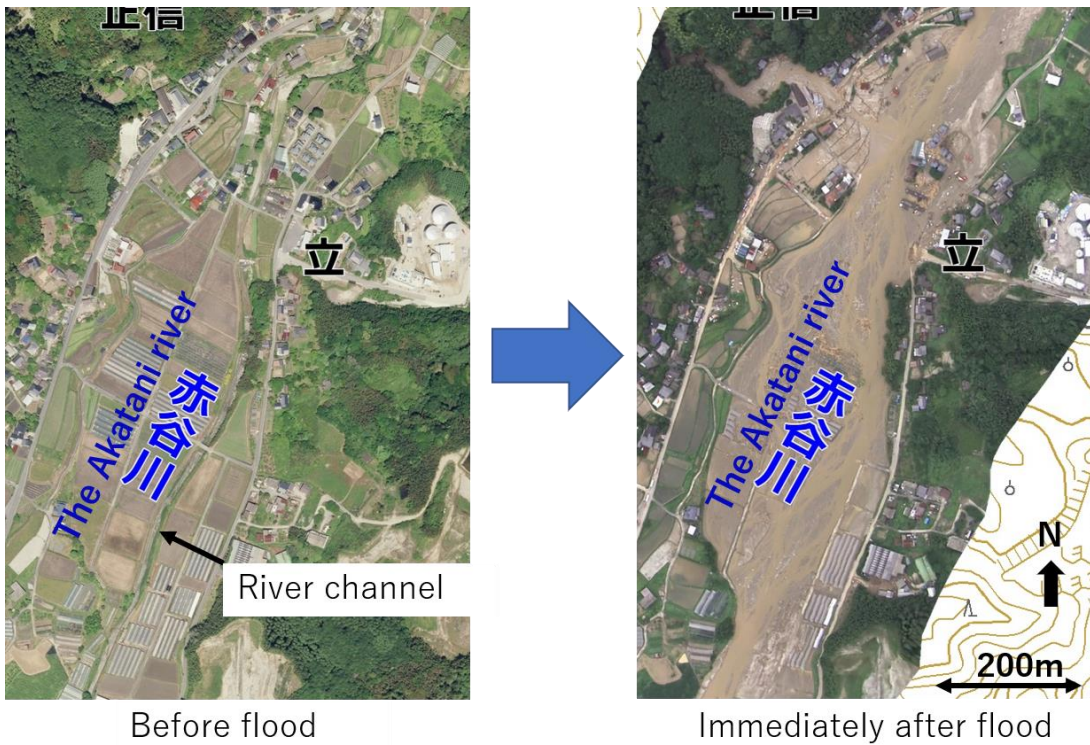
h : Depth(m) d : Diameter of driftwood

400

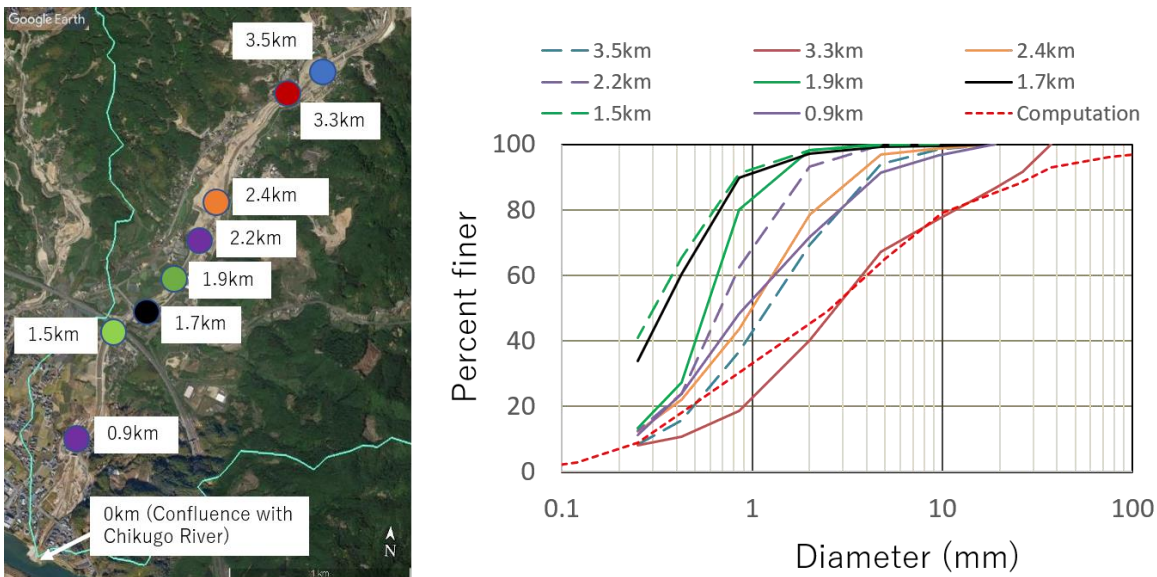
Figure 3: Specification of the functional form of $r(t, x, y)$



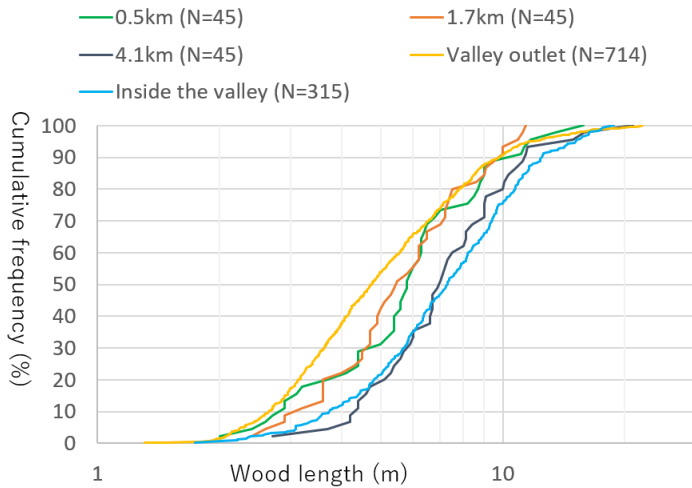
405 **Figure 4: The Akatani River basin with debris flows and flood marks identified from aerial photos (Nagumo et al., 2019 was modified by the authors). The background image is provided by the Geographical Information Authority of Japan. The debris flows and flood marks are color-coded to identify the tendency of sediment supply: (1) is along the channels, (2) is the left bank side of the Akatani river basin, (3) is the right bank side of the Otoishi river basin, (4) is the right bank side of the Akatani river basin, (5) is the Oyama river basin, (6) is the left bank side of the Otoishi river basin, and (7) is the right bank side of the Akatani river basin.**



410 **Figure 5:** Aerial photos of the Akatani River before (left) and after (right) the flood event in July 2017. The background image provided by the Geographical Information Authority of Japan.



415 **Figure 6:** Sediment sampling sites (left photo) and the sediment size distribution observed immediately after the flood event (right figure). The longitudinal distance corresponds to that of Figure 4. The green line in the left figure shows the basin boundary. The red dotted line in the right figure is employed as the initial condition in the computation. The background image was taken from © Google Maps.



420 **Figure 7: Distribution of wood length identified from aerial photos taken just after the event. Location of the valley is shown in Figure 4. The identified wood length is shown as cumulative curves.**

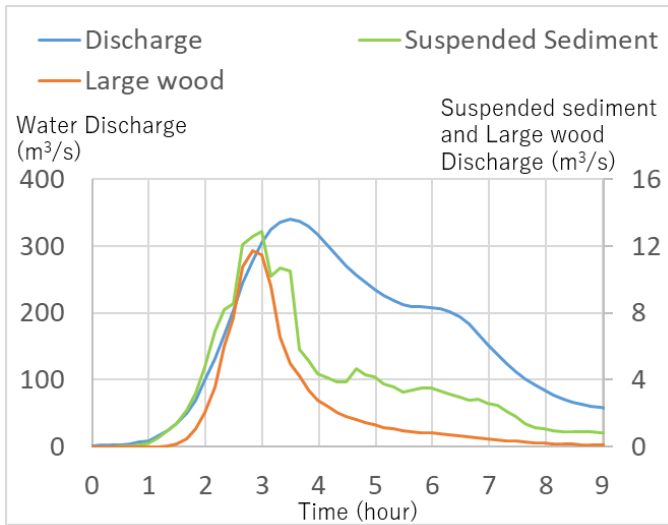


Figure 8: Computed results, i.e., upstream boundary conditions for 2-D computation, for flood water, suspended sediment, and large wood discharge at the 3.5 km point.

425

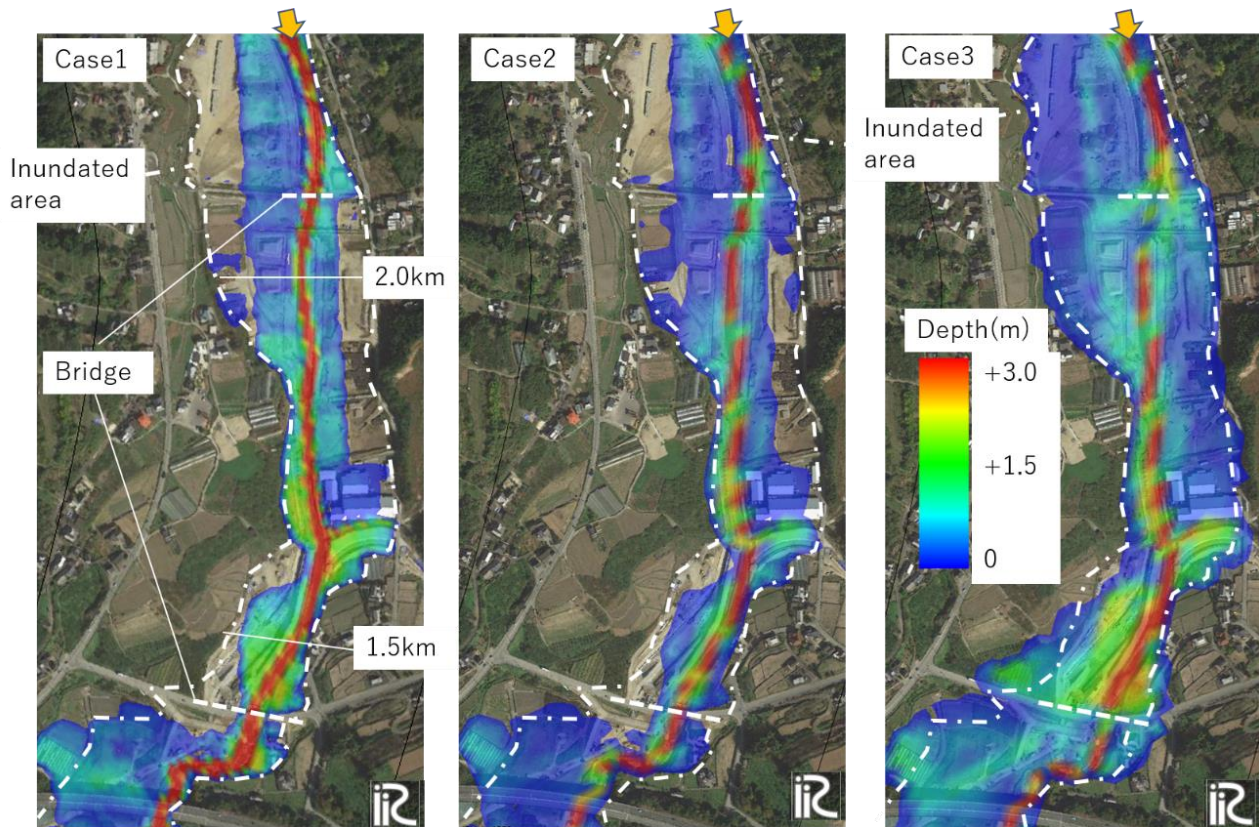
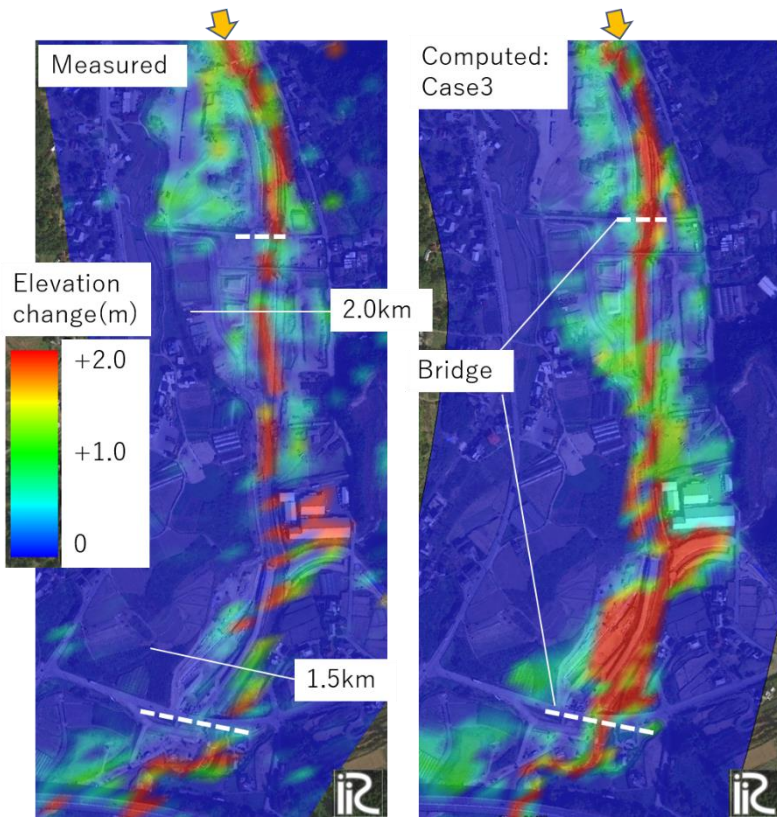
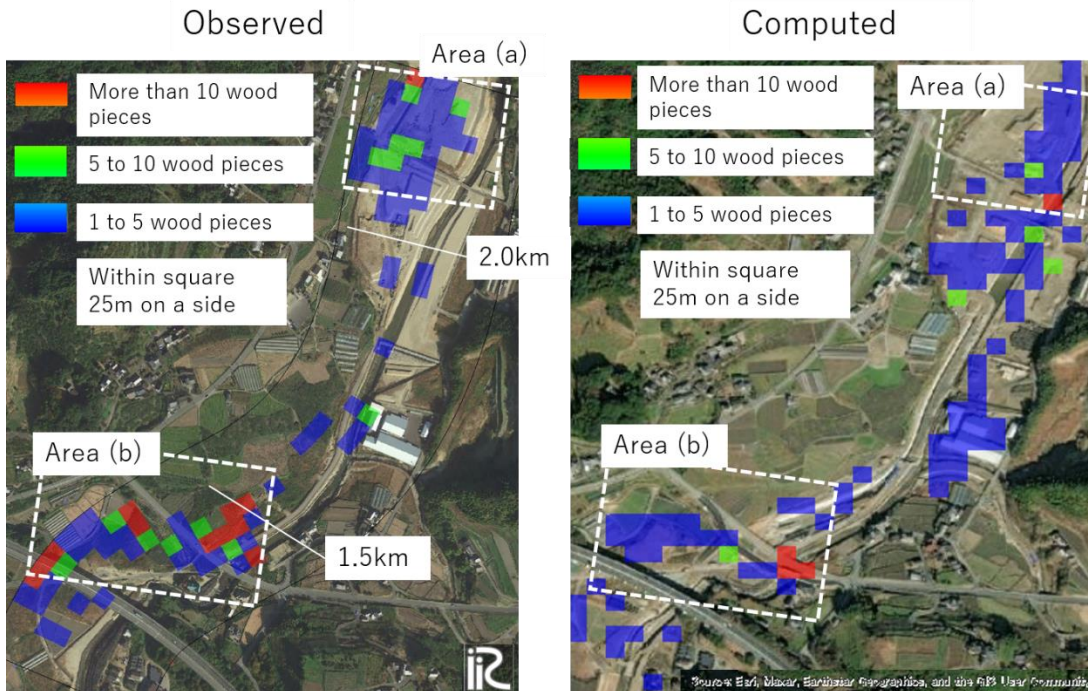


Figure 9: Comparison of water depth at peak discharge between Case 1 (left) , Case 2 (middle), and Case 3 (right). Case 1 is the flow only, Case 2 is flow with sediment without large wood, and Case 3 is flow with sediment and large wood. The white dotted line indicates the inundated area as deciphered from aerial photo. The background image was taken from © Google Maps.



430

Figure 10: Comparison of elevation changes before and after the flooding measured by aerial laser survey (left) and elevation change at the end of Case 3 calculation (right). The background image was taken from © Google Maps.



435 **Figure 11: Comparison of the large wood deposition between the observed from the aerial photos (left) and computed results (right). The computed results are converted to the number of pieces of large wood pieces by assuming that the diameter and length of a piece of wood are 20 cm and 7 m, respectively. The background image was taken from © Google Maps.**

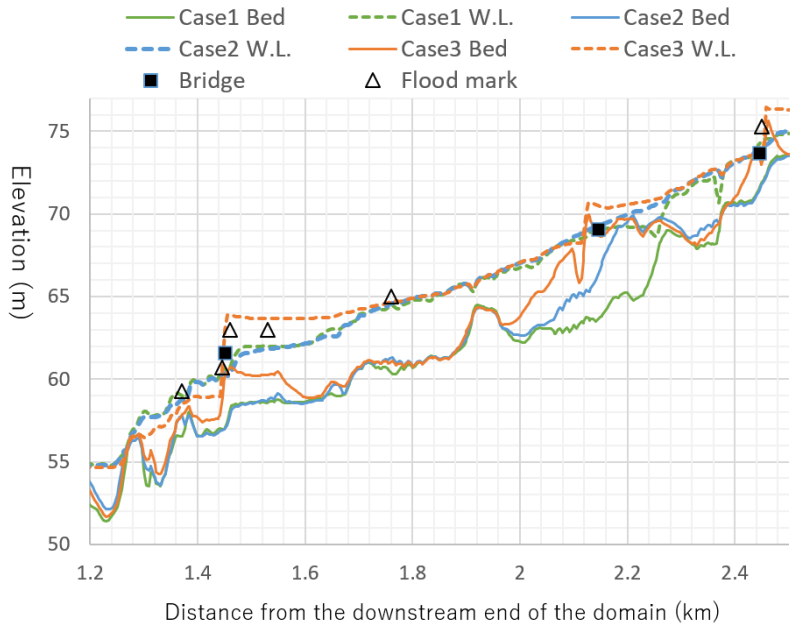
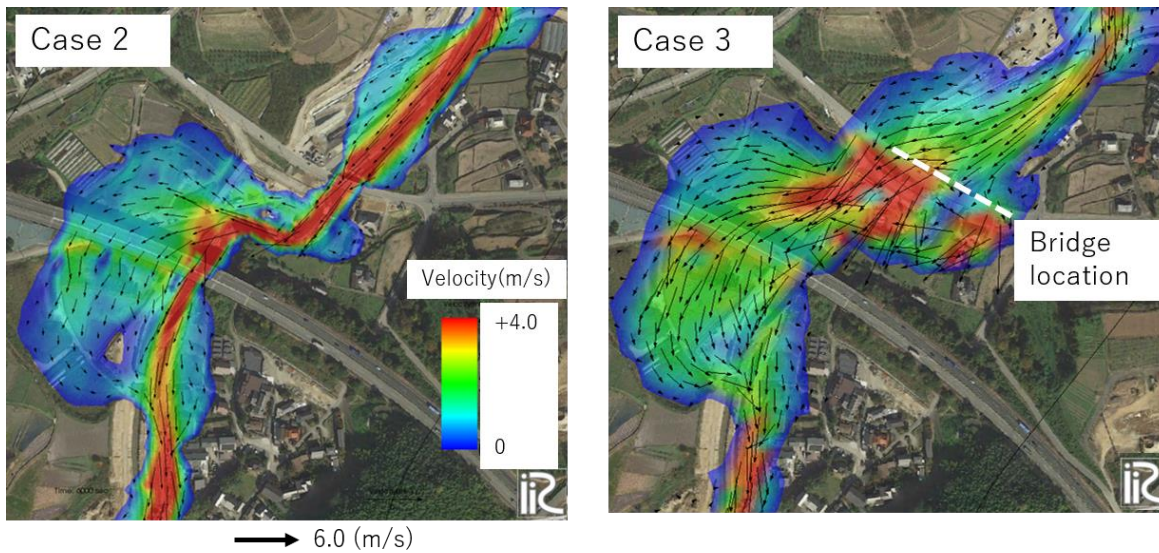


Figure 12: Comparison of the results of each case with the water level mark and river bed elevation in the longitudinal direction of the river channel during peak flow. Bridge location ■ shows the elevation of the bridge height.



440

Figure 13: Difference in flow pattern between Case 2 (left) and Case 3 (right) around the bridge at peak discharge. The background image was taken from © Google Maps.

Table 1. Parameters employed for the rainfall-runoff and landslide computations.

Item	Value
Mesh size (m)	10×10
Soil depth (m)	1.0
Saturated hydraulic conductivity (cm/s)	0.5
Equivalent roughness coefficient	0.4
Soil porosity: λ	0.475
Internal friction angle (degrees)	35
Cohesion (kN/m ²)	12.5
Soil density (kg/m ³)	2650
Water density (kg/m ³)	1000

445 **Table 2. Calculation conditions for the 2-D flood flow with sediment and large wood**

Case 1	Flow only
Case 2	Flow with sediment, without large wood
Case 3	Flow with sediment and large wood